Three-Dimensional Cross-Linked F-Actin Networks: Relation between Network Architecture and Mechanical Behavior

E. M. Huisman, T. van Dillen, P. R. Onck, and E. Van der Giessen
Micromechanics of Materials, Zernike Institute for Advanced Materials, University of Groningen, Nijenborgh 4, NL-9747 AG Groningen, The Netherlands
(Received 3 May 2007; published 14 November 2007)

Numerical simulations are reported for the response of three-dimensional cross-linked F-actin networks when subjected to large deformations. In addition to the physiological parameters such as actin and cross-linker concentration, the model explicitly accounts for filament properties and network architecture. Complementary to two-dimensional studies, we find that the strain-stiffening characteristics depend on network architecture through the local topology around cross-links.

DOI: 10.1103/PhysRevLett.99.208103 PACS numbers: 87.16.Ka, 87.15.La, 82.35.Lr

There is much interest in the mechanical properties of biological tissues and cells, e.g. [1]. One of the most prevalent protein filaments in eukaryotic cells is F-actin that, when partially cross-linked, defines the actin cortex, providing the cell's mechanical stability during cell motility. When subjected to deformation, such cross-linked biopolymer networks stiffen at increasing strain, enhancing the energy needed for further deformation [2]. Theoretical studies of this strain-stiffening response consider networks comprising infinitely many filaments that, as the sample is deformed, distort in an affine manner [3,4]. However, numerical studies of discrete networks in two dimensions do show nonaffine behavior at low and intermediate densities [5–7].

Three-dimensional (3D) biophysical networks are even richer in behavior. This Letter presents the first computational studies of the large-strain mechanical response of discrete, 3D networks of cross-linked actin filaments. We will demonstrate, for example, that 3D network behavior not only depends on measurable quantities such as actin concentration and cross-link density but also on network architecture, for instance through the connectivity and the filament length. The networks are generated by a procedure inspired by molecular dynamics, after which they are deformed using an updated-Lagrangian finite-element model. The generation starts by placing straight filaments of length L_0 at random positions and orientations inside a fully periodic unit cell of dimension W. Each filament is divided into Euler-Bernoulli beam elements, accounting for bending (stiffness κ), twisting (stiffness ω) and stretching (stiffness μ). A $1/r^p$ ($p \approx 2$) attractive force field between filaments a distance r apart initiates their movement. Damping by drag of filaments in the surrounding fluid and internal damping of filaments are taken into account for numerical convenience. When two nodes (end points of elements) approach each other within a certain cutoff distance, a rigid cross-link of zero length is formed between these nodes. Nodes are prevented to form multiple cross-links. This procedure enables us to generate networks of realistic architectures, with control over actin and cross-link concentration as well as network topology, by varying the force-field properties. To mimic physiological situations, we take $L_0 = 0.5$ to 2 μm, the actin concentration c_a around 1.5 mg/ml and the average distance between cross-links, l_c, between 0.2 and 0.3 μm [8]. Figure 1 shows a cross-linked network with $c_a = 1.56$ mg/ml. After generation, any loose ends are removed resulting in cross-links that connect either 2, 3, or 4 elements [see Fig. 1(b)].

Since *in vivo* actin networks are immersed in the cytosol, segments connecting the cross-links undergo thermally excited bending motions. As a consequence, the filaments are undulated, reducing the longitudinal stiffness of the segments compared to the filament's stretching stiffness. The key parameter determining the amplitude of the un-

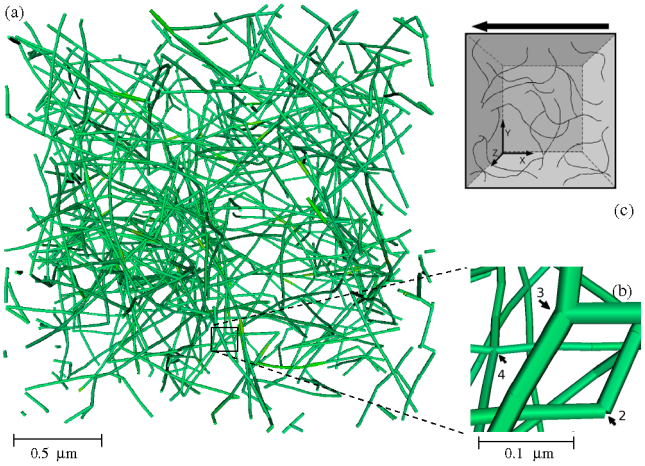

FIG. 1 (color online). 3D discrete network model of cross-linked filaments. (a) View of a network with filaments of initial length 1.3 μm, actin concentration 1.56 mg/ml, and average cross-link distance $l_c = 0.254$ μm (59.6 cross-links/μm^3, 1.95 cross-links/filament). The filament radius is magnified for plotting reasons. (b) Zoom-in of a part of the network in (a), displaying cross-links that connect 2, 3, and 4 elements. (c) Schematic representation of the network in (a), with the arrow indicating the direction of the applied shear displacement in the xy plane.

dulations is the persistence length l_p, defined as $l_p = \kappa/k_BT$ in terms of Boltzmann's constant k_B and temperature T. To account for the initial configuration of the undulated network, segments between cross-links are first straightened after the network generation and then transverse deflections are added normal to the segment. These deflections are introduced in two mutually orthogonal directions using a superposition of ten normal modes of the form $b_n \sin(n\pi x/L)$ where L is the length of the segment, x is the coordinate along the end-to-end direction of the segment and the amplitudes b_n follow a Gaussian distribution with standard deviation $\sqrt{2/(l_pL)}(L/n\pi)^2$ [5,7]. The resulting stress-free network serves as a representative volume element (RVE) of the complete network that is next subjected to a macroscopic shear of strain Γ [see Fig. 1(c)]. Throughout the article we will use experimentally obtained values of the filament's mechanical moduli, i.e., stretching stiffness $\mu = \mu_{\text{ref}} = 4.0 \times 10^{-8}$ N [9], bending stiffness $\kappa = \kappa_{\text{ref}} = 6.75 \times 10^{-26}$ N m^2 [10] and torsional stiffness $\omega = \omega_{\text{ref}} = 2.8 \times 10^{-26}$ N m^2 [11], unless stated otherwise. Convergence studies ensured that the cell size ($W = 2.5$ μm) and the length of the beam elements (0.1 μm) do not affect the results. During mechanical loading, undulation dynamics and viscous drag are not taken into account.

Figure 2 shows the network of Fig. 1 at three stages of strain. The color of each element is related to the relative energy difference between the bending energy E_{bn} and stretching energy E_{ax}, defined, respectively, as $E_{\text{bn}} = \int \frac{1}{2}\kappa(\phi')^2 ds$ and $E_{\text{ax}} = \int \frac{1}{2}\mu(u')^2 ds$ in which ϕ' is the curvature and u' is the axial strain along the element, both parametrized by the arc length s. The torsional energy

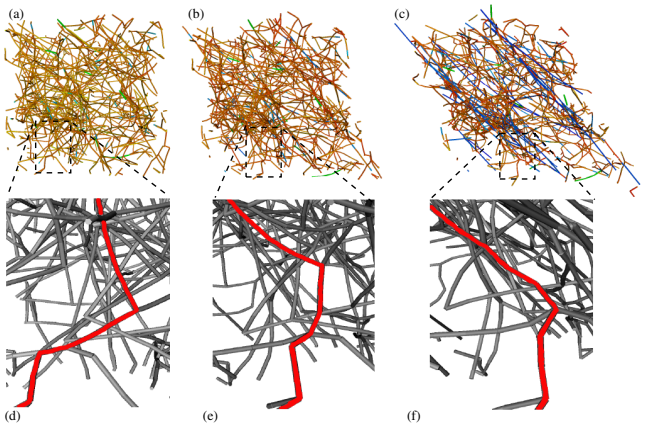

FIG. 2 (color online). Network of Fig. 1 under shear at different strain levels. (a) $\Gamma = 0.1$, (b) $\Gamma = 0.3$ and (c) $\Gamma = 0.5$. The color of each element corresponds to the value of the normalized energy difference $(E_{\text{ax}} - E_{\text{bn}})/\bar{E}$ (< 0 red; ≈ 0 green; > 0 blue), where E_{ax} and E_{bn} are the axial stretching energy and bending energy, respectively, and $\bar{E}$ is the network's total energy at each strain level. The lower-left region of the RVE is enlarged in (d),(e),(f) to highlight a network section (in red) that reorients and stretches under deformation. Views from other directions can be found in [17].

is ignored, since it is negligibly small (the total torsional energy is 2% of the total energy at $\Gamma = 0.1$, 0.5% at $\Gamma = 0.3$ and only 0.01% at $\Gamma = 0.5$). At small strains, most elements in the network are in a state of bending. However, as the network deforms, filaments reorient in the direction of straining by rotation and translation, resulting in percolations of stretched out filaments connecting the top and bottom of the RVE. This is seen in Fig. 2(c) by the strings of blue elements. The reorientation of filaments can be viewed by zooming into the network, Figs. 2(d)–2(f). The highlighted red section reorient at intermediate strains ($\Gamma < 0.3$) and stretches at larger strains.

The solid curve in Fig. 3(a) shows the calculated shear stress τ (in Pa) of the particular actin network as a function of strain Γ. At small strains the network response is linear with a shear stiffness of 26 Pa, which is comparable to measured stiffnesses of similar networks [4,12]. The stiffness gradually increases at intermediate strains to a value of 430 Pa at $\Gamma = 0.35$ and around 1400 Pa at $\Gamma = 0.45$, see Fig. 3(b). Next, we have increased the stretching stiffness μ by 1 order of magnitude, leaving the bending and torsional stiffnesses (κ and ω) unchanged. The dashed curve in Fig. 3(a) shows that up to $\Gamma \approx 0.28$ the response is identical to that of the reference network (solid line); for $\Gamma > 0.4$, the slope increases as a direct result of the larger value of μ. However, in case the bending stiffness is reduced by a factor 3 (while keeping μ and ω unchanged), it is the small-strain response that is different, as can be seen from the dash-dotted curve in Fig. 3(a). These observations again demonstrate the existence of three strain regimes, i.e., a small-strain bending-dominated regime, an intermediate-strain transition regime, and a large-strain stretching-dominated regime, in accordance with the snapshots displayed in Fig. 2. The three regimes can be clearly distinguished by noting from the inset of Fig. 3(a) that the network's total bending energy, $\bar{E}_{\text{bn}}$ dominates at small strains, whereas $\bar{E}_{\text{ax}}$ dominates at large strains.

The discrete network model allows us to separately study the effect of filament undulations. To this end, we compare the results presented so far with the response of the networks comprising straight segments between cross-links. It is noted, however, that by ignoring the undulation dynamics, our model accounts for only half (initially) to one fourth (at large strains) of the entropic stiffness [7]. Since the axial stiffness is underestimated, the network response is a lower bound to the actual network response. The amplitude of the undulations depends on l_c and $l_p = \kappa/k_BT$, the latter being around 17 μm at room temperature for κ_{ref}. Thus, for physiologically relevant networks such as the reference network (Fig. 1), the persistence length is much larger than the average length of segments between cross-links. Figure 3(b) shows the influence of undulations on the response for both $l_p \approx 70 l_c$, representative for the networks shown in Figs. 1 and 2, and $l_p \approx l_c$ (obtained by reducing the value of κ). As a reference, the response of networks with straight filaments between the cross-links is

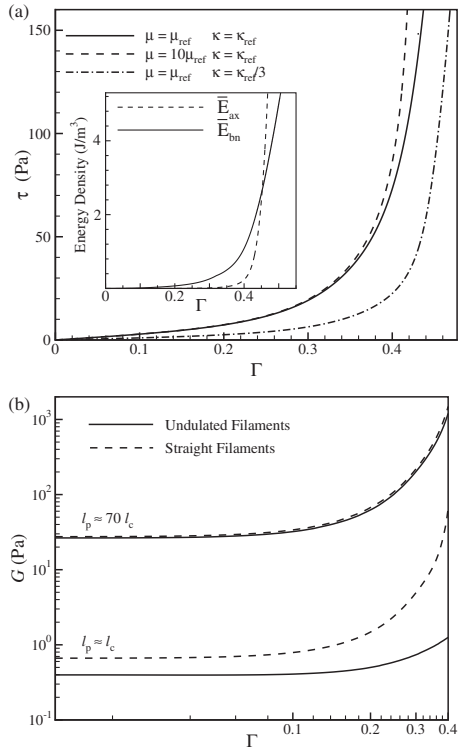

FIG. 3. Predicted overall response of F-actin networks. The shear stress τ versus shear strain Γ response is shown in (a) for different values of μ and κ (ω is left unchanged), and reveals that the small-strain response is governed by the bending stiffness κ. The inset shows the overall axial and bending energy densities $\bar{E}_{\mathrm{ax}}$ and $\bar{E}_{\mathrm{bn}}$, respectively, as a function of Γ for the solid curve in (a). (b) Overall network stiffness of networks with straight (dashed curves) and undulated (solid curves) segments between filaments.

included. Clearly, for $l_p \gg l_c$, the sections between cross-links are virtually straight, explaining the correspondence with the network comprising straight filaments. However, a network with $l_p \approx l_c$ has a significant slack, giving rise to a softer response than that of straight-filament networks. Note that $l_p \approx l_c$ is representative for low density networks consisting of "floppy" filaments such as fibrin or vimentin.

Interestingly, the stress-strain response of the reference network [see Fig. 3(b)] has the same overall shape as experimentally measured responses of actin networks [8,13] up to strains where networks start to soften, e.g., due to rupture. Unfortunately, a quantitative comparison to experiments is hampered by the many experimental uncertainties in the cross-link distance and in the filament length, parameters that we will now show to have a major influence.

We proceed by showing that the response strongly depends on the network architecture, something that exists predominantly in 3D. Networks of constant initial concentration, $c_a = 1.2$ mg/ml, and constant cross-link distance, $l_c = 0.3$ μm, were generated using filaments of different initial length L_0. Figure 4(a) shows the corresponding dependence of the initial stiffness $G_0 = d\tau/d\Gamma$ (at $\Gamma = 0$) on L_0. As can be seen, the stiffness strongly increases with the length of the filaments, even though the concentration and cross-link distance are constant. This increase originates from a change in the network topology, as can be concluded from the distribution in cross-link connectivity (2, 3 or 4 cf. Fig. 1) for several values of L_0 plotted in Fig. 4(b). Clearly, networks generated with longer filaments show a decrease in cross-link connectivity of 2 and 3, and an increase in connectivity of 4, thus resulting in a stiffer network structure, as seen in Fig. 4(a).

We have also explored the effect of varying l_c and c_a for a given length L_0. To avoid that the network topology is changed at the same time, we scale up one of the networks having $L_0 = 1.2$ μm of Fig. 4(a) by different factors. This yields networks of identical architecture, but of different $c_a \propto l_c^{-2}$. In Fig. 4(a) the calculated G_0 is plotted as a function of l_c (triangles). The dashed line is a power-law fit $G_0 \propto l_c^q$ with exponent $q \approx -4.0$ (or $G_0 \propto c_a^p$ with $p \approx 2.0$) which is expected for networks with straight segments [8,14]. These results are hard to obtain in experiments, since there l_c and c_a cannot be varied independently from the network topology.

Finally, we have investigated the deviation from affinity of deformation. A network of concentration 1.3 mg/ml was subjected to a shear strain Γ in the xy-plane. Figure 5(a) shows the trajectories of cross-links (20% is

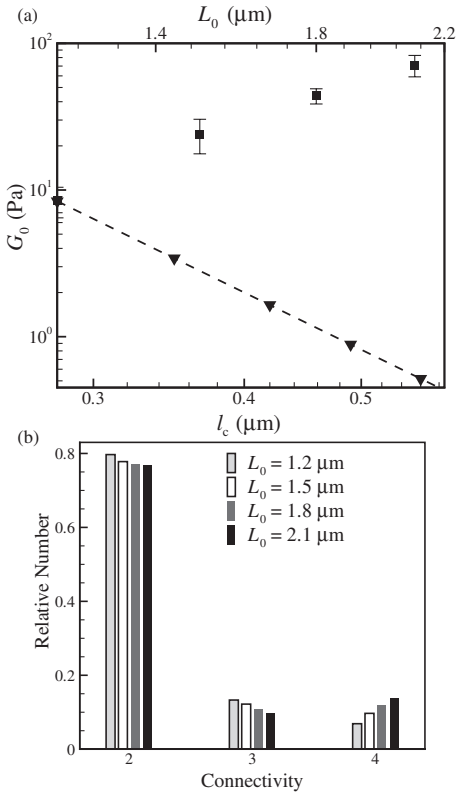

FIG. 4. Influence of network architecture on the mechanical response. (a) Initial stiffness G_0 versus initial filament length L_0 (squares) and versus l_c (triangles). The error bars indicate the variation in the response of 10 different random realizations of networks. (b) Cross-link connectivity distribution for several lengths of filaments.

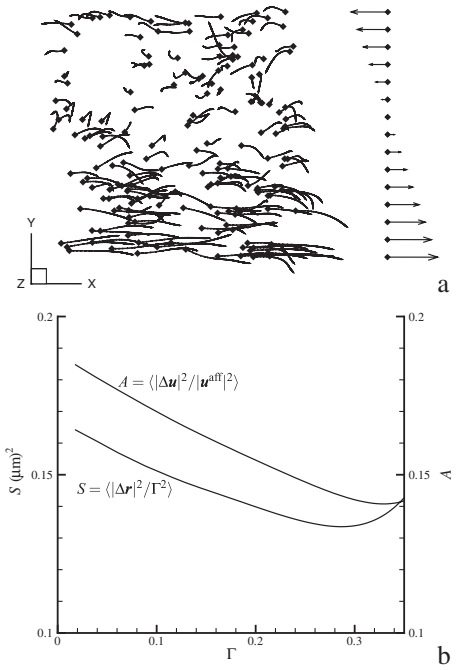

FIG. 5. The distortion of a cross-linked network is nonaffine as revealed by the trajectories in the xy plane of 20% of all cross-links during shearing from $\Gamma = 0.0$ (diamonds) to $\Gamma = 0.35$ (a) and by the scalar measures S and A of affinity (b). Animations of the motion can be found in [15].

plotted) projected onto the xy-plane. The diamonds indicate the starting positions of cross-links and each trajectory stops at a macroscopic strain of $\Gamma = 0.35$. As a reference, the expected affine shear motion as a function of height y is indicated by the arrows on the right-hand side of the figure. Not shown, but available in [15], are the nonaffine motions normal to the shearing plane. The deviation from affine behavior varies with deformation, as shown in Fig. 5(b) for two measures of nonaffinity. The parameter S measures the mean deviation $\Delta \boldsymbol{r}$ from the affine position of the cross-link for each strain, and was used very recently by Liu *et al.* [16] in experiments where probe particles were embedded to measure the nonaffinity during in-vitro shear experiments. Especially when taking into account that the average spacing between 20% of the cross-links is smaller than that between the markers in [16], our predicted values are somewhat smaller than the experimental values for networks with comparable stiffening. Contrary to S, the second nonaffinity measure shown, A, is dimensionless, monitors the difference in the cross-link displacement $\boldsymbol{u}$ and is related to the one we used previously in two dimensions [5]. On the basis of this information and additional simulations we can conclude that the local deformation is nonaffine, even at densities as high as 4.0 mg/ml. Three dimensionality imposes fewer constraints on the deformation of filaments, and thus extends the range of nonaffinity as compared to the 2D case.

Next to the actin concentration and distance between cross-links, the local topology around cross-linkers is a key ingredient for the overall network stiffness. It should be noted that in this work the cross-links are rigid, so that all degrees of freedom of the filaments are rigidly connected. Actual cross-binding proteins are likely to impose a less severe constraint on the filaments, which is expected to result in a more compliant response. The fact that network topology depends on filament length partly explains the role of length controlling proteins (gelsolin, capZ) used by the cell to modify cytoskeletal actin networks during, e.g., cell locomotion. Small changes in the concentration of these proteins can induce large changes in stiffness. The large influence of actin binding proteins on the network response [8,13] might not only be caused by their intrinsic properties, but also by the influence of these binding proteins on the network topology. Since the properties and dynamical characteristics of cross-links can well be incorporated into the model, this technique will provide a powerful tool to gain more insight into fundamental, biomechanical processes in cells and tissues, such as mechanotransduction, cell division, and motility.

[1] K. E. Kasza, A. C. Rowat, J. Liu, T. E. Angelini, C. P. Brangwynne, G. H. Koenderink, and D. A. Weitz, Curr. Opin. Cell Biol. **19**, 101 (2007).
[2] N. Wang and D. E. Ingber, Biochemistry and Cell Biology **73**, 327 (1995).
[3] F. C. MacKintosh, J. Käs, and P. A. Janmey, Phys. Rev. Lett. **75**, 4425 (1995).
[4] C. Storm, J. J. Pastore, F. C. MacKintosh, T. C. Lubensky, and P. A. Janmey, Nature (London) **435**, 191 (2005).
[5] P. R. Onck, T. Koeman, T. van Dillen, and E. Van der Giessen, Phys. Rev. Lett. **95**, 178102 (2005).
[6] D. A. Head, A. J. Levine, and F. C. MacKintosh, Phys. Rev. Lett. **91**, 108102 (2003).
[7] T. van Dillen, P. R. Onck, and E. van der Giessen, arXiv:physics/0611230.
[8] M. L. Gardel *et al.*, Proc. Natl. Acad. Sci. U.S.A. **103**, 1762 (2006).
[9] X. M. Liu and G. H. Pollack, Biophys. J. **83**, 2705 (2002).
[10] A. Ott, M. Magnasco, A. Simon, and A. Libchaber, Phys. Rev. E **48**, R1642 (1993).
[11] R. Yasuda, H. Miyata, and K. Kinosita, J. Mol. Biol. **263**, 227 (1996).
[12] P. A. Janmey, S. Hvidt, J. Lamb, and T. P. Stossel, Nature (London) **345**, 89 (1990).
[13] R. Tharmann, M. M. A. E. Claessens, and A. R. Bausch, Phys. Rev. Lett. **98**, 088103 (2007).
[14] L. J. Gibson and M. F. Ashby, *Cellular Solids: Structures and Properties* (Pergamon, Cambridge, 1988).
[15] See EPAPS Document No. E-PRLTAO-99-031745 for animations of the cross-link motions corresponding to Fig. 5(a). For more information on EPAPS, see http://www.aip.org/pubservs/epaps.html.
[16] J. Liu *et al.*, Phys. Rev. Lett. **98**, 198304 (2007).
[17] See EPAPS Document No. E-PRLTAO-99-031745 for views of Fig. 2 from all three directions. For more information on EPAPS, see http://www.aip.org/pubservs/epaps.html.